

Second harmonic generation of GaN(0001)

V. I. Gavrilenko

Rudolph Technologies Inc., Flanders, New Jersey 07836

R. Q. Wu

Department of Physics and Astronomy, University of California, Irvine, California 92697

(Received 6 April 2001; published 19 December 2001)

Second harmonic generation (SHG) spectra of the Ga- and N-terminated GaN(0001) surfaces have been studied by using the first-principles full potential linearized augmented plane-wave method. Equilibrium surface geometries are determined through the total-energy minimization method. The calculated SHG spectra in the low-energy spectral range are dominated by the two-photon resonances associated with the surface states, while in the high energy range the SHG responses are contributed from the bulk states. Adsorption of Ga on the N-terminated GaN(0001) surface results in a substantial evolution of the surface related SHG features.

DOI: 10.1103/PhysRevB.65.035405

PACS number(s): 78.66.-w, 42.65.Ky, 73.20.-r

I. INTRODUCTION

GaN is a promising material for various technological applications, such as short-wavelength light emitting diodes, semiconductor lasers, and optical detectors, etc.^{1,2} Second harmonic generation (SHG) (Refs. 3–10) as surface-specific optical spectroscopy has been applied to different semiconductor-atom systems. From a practical standpoint, their noninvasive nature, high sensitivity to submonolayer adsorption, and strong dependence of the spectroscopic response on the adatom species have proven extremely useful for real time, *in situ* monitoring of surface dynamic processes involving various adsorbents.³ Several SHG studies of GaN surfaces and interfaces are reported in Refs. 3, 9, and 10. On the GaN(0001) surface¹⁰ interesting optical SHG structures were reported, which could not be explained by bulk contributions.

Significant progress in quantitative theoretical explanation of surface-specific spectroscopic responses has also been made in recent years. The semiempirical tight-binding model (SETBM) of surface optics¹¹ has been used to explain SHG response from Si surfaces.^{12,13} The SETBM correctly predicted tendencies in SHG behavior for different surfaces and ambients, but it proved to be significantly less successful in quantitatively explaining nonlinear surface spectra. The reason for this is due to the well pronounced surface/interface localization of the SHG signal. Strong contribution of the surface/adsorbate specific electronic states to SHG requires additional parametrization of interatomic interactions and optical matrix elements, which usually strongly depend on the change in environment. The complex surface chemistry is certainly difficult for the SETBM based only on a few parameters. Recently we presented an *ab initio* pseudopotential approach for the SHG spectra of Si(001)-adsorbate systems,^{14,15} which reproduced well all essential features of the observed SHG spectra. Significantly, the strongly contrasting effects of H and Ge adsorbents¹⁵ and B surface doping¹⁴ on the SHG spectrum were reproduced in quantitative detail, thus testing the theory more stringently than for merely a single adsorbent. Equally important, the calculations showed that the basic adsorbate-specific trends in the

SHG spectra were rather insensitive to the accuracy of the structural optimization, but extremely sensitive to the quality of the near-surface eigenvectors and eigenstates, i.e., to the full convergence of self-consistent all-electron treatments.

In the present paper we report results of SHG for the GaN(0001) N- and Ga-terminated surfaces by using the first-principles full potential linearized augmented plane-wave (FLAPW) method. This theory has better precision for optics than the pseudopotential approaches in particular for materials with first row elements (like N). The high accuracy of the FLAPW method in predicting linear and nonlinear optical spectra of group-III nitrides was demonstrated recently in Ref. 16. Here we extend our FLAPW study to the nonlinear optics of their surfaces. The main goal of this work is to predict the surface specific features of SHG spectra of wurtzite GaN crystals. Based on comparison of the SHG spectra calculated for GaN(0001)(1×1):N and GaN(0001)(1×1):Ga surfaces, we predict changes of the SHG response by adsorption of Ga. The paper is organized as follows. In Sec. II we describe the details of the numerical method. In Sec. III, the formulation of the dipolar nonlinear optical susceptibility is given to elucidate the key points in the computational procedure of SHG. In this section we also discuss the restrictions which may apply for reliable SHG predictions on the surface. In Sec. IV we discuss our results for GaN(0001)(1×1):N and GaN(0001)(1×1):Ga surfaces in comparison with experimental data.

II. METHOD

The electronic band structure and optical function computations are based on the film-FLAPW theory.^{17,18} In the FLAPW method no shape approximation is made for charge density, potential, and matrix elements in all the three regions (vacuum, interstitial, and muffin tin).¹⁷ FLAPW calculations have provided very accurate results of linear and nonlinear optical functions for different $A^{III}B^V$ compound semiconductors (see, e.g., Ref. 16 and references therein).

Equilibrium surface geometries are determined through total-energy minimization guided by atomic forces. Calculations of electronic-structure and optical properties are based

on the generalized gradient approximation (GGA).¹⁹ Eigenvalues and wave functions are obtained by direct diagonalization of the Hamiltonian with the fully converged charge density. We modeled the surface by a slab containing eight GaN monolayers (ML's). Test calculations with a thicker slab (up to 16 GaN ML's) indicate that the results reported here are reliable within 10–15%.

To compare with experiments, the quasiparticle (QP) corrections are usually invoked in most theoretical papers through a scissorslike operator. The value of the energy shift Δ_{QP} was chosen to match the experimental gap energy E_g . Due to the strong \mathbf{k} dependence of Δ_{QP} (see, e.g., Ref. 20 and references therein), however, this treatment does not improve deviations between the calculated and measured optical functions in the high-energy spectral region. The reason for this is that the scissorslike corrections do not improve the bandwidth of the conduction band (c band). The GW corrections,^{21,22} which are beyond the scope of this paper, are needed for a better quantitative comparison with experiments. In addition, the scissorslike QP corrections do not apply for cases with half filled metallic bands as found for the GaN(0001) surfaces. Therefore no QP correction is adopted here.

III. NONLINEAR OPTICAL SUSCEPTIBILITY

Calculations of optical functions are based on a single-electron picture without the excitonic and local-field corrections. The polarization P of a solid induced by an incident harmonic radiation at frequency ω can be expanded up to the second order in electric field of light as

$$P_i(\mathbf{r}, \omega) = \chi_{ij}^{(1)} E_j(\mathbf{r}, \omega) + \chi_{ijk}^{(2)} E_j(\mathbf{r}, \omega) E_k(\mathbf{r}, \omega) + Q_{ijkl}^{(2)} E_j(\mathbf{r}, \omega) \nabla_k E_l(\mathbf{r}, \omega), \quad (1)$$

where optical susceptibility functions $\chi^{(1)}$ and $\chi^{(2)}$ stand for the linear and nonlinear responses, respectively, and $Q^{(2)}$ describes the quadruple contribution to P .

A. Microscopic formulation

The ensemble average polarization P of the system is determined through the density matrix (ρ):

$$\langle \mathbf{P} \rangle = \text{Tr}(\rho \mathbf{P}). \quad (2)$$

The time-dependent response of a system to the incident harmonic radiation is determined by the equation of motion for ρ , which at the thermal equilibrium is given by²³

$$\frac{\partial \rho}{\partial t} = \frac{1}{i\hbar} [H_o + V, \rho], \quad (3)$$

where H_o is the Hamiltonian of the unperturbed solid, and V describes the interaction between the radiation and the matter. Equation (3) can be projected on the orthogonal Bloch eigenfunctions $|s\rangle$ of H_o , $[(H_o - E_s)|s\rangle = 0]$. In the thermodynamic equilibrium, the density matrix in the single-electron picture is defined through the Fermi distribution function, $f_o(E_s) = \{\exp[(E_s - F)/kT] - 1\}^{-1}$, as²³

$$\rho_{i,j}^{(0)} = f_o(E_i) \delta_{ij}.$$

At zero temperature [with $f_o(E_{s'}) = 1$ for the occupied (v) states and $f_o(E_s) = 0$ for the empty (c) states], the first and second order solutions of Eq. (3) for harmonic radiation, $V(t) = V_o \exp(-i\omega t)$ are given by

$$\rho_{s,s'}^{(1)} = \frac{V_{s,s'}}{E_s - E_{s'} - \hbar\omega}, \quad (4)$$

$$\rho_{s,s'}^{(2)} = \frac{1}{E_s - E_{s'} - \hbar\omega} \sum_{s''} \langle s|V|s''\rangle \langle s''|V|s'\rangle \times \left(\frac{1}{E_{s''} - E_{s'} - \hbar\omega} - \frac{1}{E_s - E_{s''} - \hbar\omega} \right). \quad (5)$$

B. Second-order nonlinear optical susceptibilities

Equations (1), (2), and (5) can be used now to derive the expression for $\chi^{(2)}$. To this end one should specify the perturbation term in Eq. (3) which can be used in the form of $V = -e/mc \mathbf{A} \mathbf{p}$ (velocity gauge) or $V = -e \mathbf{E} \mathbf{r}$ (length gauge). In a frequency range below near ultraviolet the light wave vector is vanishingly small, therefore both approaches yield the same results.²⁴ In a series of papers, Levine and Allan²⁵ as well as Del Sole and Girlanda²⁶ demonstrated how to use the length gauge for the determination of optical susceptibilities. Equations (1)–(5) in the length gauge yield the well-known formula for $\chi^{(2)}$ given in many books for nonlinear optics.^{27–29} To avoid the divergence, the diagonal ($s = s'$) terms for the intraband transitions need to be excluded. It has been shown for bulk SHG that these terms provide insignificant contributions to $\chi^{(2)}$ and thus can be omitted in most cases.^{24,30} According to our recent finding,¹⁵ however, the intraband contributions become more important for the determination of surface SHG. Sipe and Ghahramani³¹ derived equations invoking explicitly both the inter- and intraband contributions. Using the latest formalism in the length gauge (atomic units), the $\chi_{ijk}^{(2)}(-2\omega, \omega, \omega)$ is given by³²

$$\chi_{ijk}^{(2)}(-2\omega, \omega, \omega) = \int \frac{d\mathbf{k}}{4\pi^3} [\chi_{ll}^{ijk}(-2\omega, \omega, \omega) + \eta_{ll}^{ijk}(-2\omega, \omega, \omega) + \sigma_{ll}^{ijk}(-2\omega, \omega, \omega)], \quad (6)$$

$$\chi_{ll}^{ijk}(-2\omega, \omega, \omega) = \sum_{nml} \frac{r_{nm}^i \{r_{ml}^j r_{ln}^k\}}{\omega_{ln} - \omega_{ml}} \left(\frac{2f_{nm}}{\omega_{mn} - 2\omega} + \frac{f_{ml}}{\omega_{ml} - \omega} + \frac{f_{ln}}{\omega_{ln} - \omega} \right), \quad (7)$$

$$\begin{aligned}
& \eta_{ll}^{ijk}(-2\omega, \omega, \omega) \\
&= \sum_{nml} \left[\omega_{nm} r_{nm}^i \{r_{ml}^j r_{ln}^k\} \left(\frac{f_{nl}}{\omega_{ln}^2(\omega_{ln} - \omega)} - \frac{f_{lm}}{\omega_{ml}^2(\omega_{ml} - \omega)} \right) \right. \\
&\quad \left. + 2 \frac{f_{nm} r_{nm}^i \{r_{ml}^j r_{ln}^k\} (\omega_{ml} - \omega_{lm})}{\omega_{mn}^2(\omega_{mn} - 2\omega)} \right] - 8i \sum_{nm} \frac{f_{nm} r_{nm}^i \{\Delta_{nm}^j r_{nm}^k\}}{\omega_{mn}^2(\omega_{mn} - 2\omega)}, \quad (8)
\end{aligned}$$

$$\begin{aligned}
& \sigma_{ll}^{ijk}(-2\omega, \omega, \omega) \\
&= \sum_{nml} \frac{f_{nm}}{\omega_{mn}^2(\omega_{mn} - \omega)} [\omega_{nl} r_{lm}^i \{r_{mn}^j r_{nl}^k\} - \omega_{lm} r_{nl}^i \{r_{lm}^j r_{mn}^k\}] \\
&\quad - i \sum_{nm} \frac{f_{nm} \Delta_{nm}^i \{r_{mn}^j r_{nm}^k\}}{\omega_{mn}^2(\omega_{mn} - \omega)}, \quad (9)
\end{aligned}$$

where $\Delta_{nm}^i \equiv p_{nn}^i - p_{mm}^i$, $\{r_{ml}^j r_{ln}^k\} \equiv \frac{1}{2}(r_{ml}^j r_{ln}^k + r_{ml}^k r_{ln}^j)$, ω_{nm} is the energy difference between levels n and m , and $f_{nm} \equiv f_n - f_m$, with f_i the Fermi occupation factor at zero temperature.³² Matrix elements \mathbf{r}_{nm} are usually evaluated through momentum matrix elements \mathbf{p}_{nm} as $\mathbf{r}_{nm} = \mathbf{p}_{nm}/im\omega_{nm}$.³²

C. Surface nonlinear optical response

The above formalism has been successfully applied recently in the SHG studies for several bulk materials.^{16,32,33} It is not a trivial task, however, to extend it for surface SHG owing to the following reasons.

(i) The lowered symmetry at surfaces induces localized surface states which, in turn, result in unusual features of optical excitations not presented in the bulk.

(ii) Structural relaxations and reconstructions cause changes of electron band structure related to the excitations of bulklike atomic orbitals in the near-the-surface region.

(iii) The normal component of the light electric field decays rapidly in the surface region (discontinuity in the classical picture).

(iv) The local-field effect and electron screening, which at surface could be different from those in bulk.

(v) The dc electric field established in the surface barrier causes electric-field induced second harmonic (EFISH) response through the third-order nonlinear contribution.

The first two points are treated well in most of modern first-principles approaches. As found in our previous calculations, the surface states induce pronounced different features below the threshold in the bulk SHG spectra. They provide additional means to monitor the surface chemistry. The surface structure relaxation and reconstruction can be determined with a high accuracy in total-energy and force optimizations. Our calculations show that the strain effect on SHG is negligible for Ge/Si(001) systems.¹⁵

The discontinuity of the z component of the light electric field gives rise to a large field gradient that can generate a sizable contribution from the quadruple terms [see Eq. (1)].^{34,35} The error associated to this effect will be enhanced if the surface states orient along the z direction. This occurs

for the N-terminated surface, where there is only one z -oriented surface state per unit cell.

The local-field effect provides 10–30% contributions to linear polarization functions of bulk semiconductors.²⁰ Effect of electron screening (more precisely the effect of electron exchange and correlation interaction on the optical polarization function) is usually less pronounced and very often compensates the local-field effect.²⁰ The local-field corrections on nonlinear optical susceptibilities were found to be in a range of -21 – $+30\%$ in bulk semiconductors.³⁶ It is reasonable to expect the same range for the surface corrections.

Electric-field effects in SHG, the EFISH, could provide substantial contribution to the surface response. The corresponding term in polarization function is described by the third-order optical susceptibility [which is not presented in Eq. (1)]. Experimental studies^{37,38} as well as theoretical estimates¹⁴ for silicon surface suggested that EFISH could even be comparable to the second (dipole) term in Eq. (1).

The latter three factors will be analyzed in our future work. In this paper, we focus on the leading dipolar contributions to SHG given in Eq. (6). The main features in the spectral region associated to excitations of bulklike states should be reliable. In the long-wave spectral region where the surface states play the key role, the calculated SHG should be viewed only qualitatively.

In the present work, contributions to \mathbf{p}_{nm} only from atoms in the upper half of the slab^{12,14} are calculated. In other words, we consider only one surface for the SHG determination.

D. SHG efficiency

In real experiment, the SHG efficiency $R(\omega)$ is measured, which is defined as³⁹

$$R(\omega) = \frac{I_r(2\omega)}{I_i^2(\omega)},$$

where indexes r and i denote reflected and incident intensities of the second harmonic fields, respectively. The function of R is a combination of different (allowed by symmetry) components of $\chi_{ijk}^{(2)}(\omega)$ and it is usually very difficult to single out these components experimentally (see, e.g., Ref. 10). Here we calculate the SHG efficiencies R_{pp} and R_{sp} for both p -polarized incoming, p -polarized outgoing (p -in/ p -out), and s -polarized incoming, p -polarized outgoing (s -in/ p -out) light geometries, respectively.

The local symmetry of the GaN(0001)(1×1) surface is C_{3v} which is a subgroup of the C_{6v}^4 spatial group of bulk GaN wurtzite crystals. Based on general rules,⁴⁰ the values of R_{pp} and R_{sp} for the C_{3v} symmetry are given by

$$\begin{aligned}
R_{pp} &= C \left| \frac{i}{n_\omega} T_p(2\omega) T_p^2(\omega) (\sin^2 \theta \chi_{zzz} \right. \\
&\quad \left. + n_{2\omega} n_\omega F^2(\omega) \chi_{zxx} - 2F(\omega) F(2\omega) \chi_{xzx} \right|^2, \quad (10) \\
R_{sp} &= C |T_p(2\omega) T_s^2(\omega) \chi_{zxx}|^2, \quad (11)
\end{aligned}$$

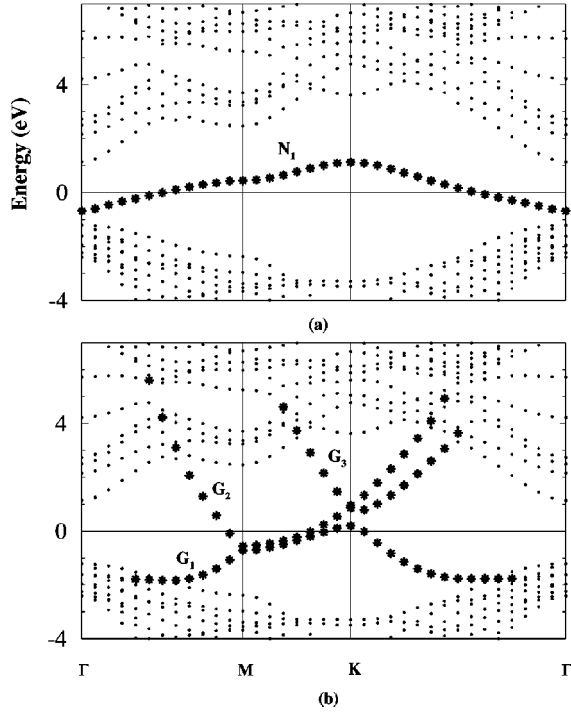


FIG. 1. The calculated electron band structure of N- (a) and Ga- (b) terminated GaN(0001)(1×1) surface.

$$C = \frac{32\pi^2 e^2}{m^2 c^3} \omega^2 \tan^2 \theta, \quad (12)$$

$$T_p = \frac{2\sqrt{\epsilon} \cos \theta}{\epsilon \cos \theta + \sqrt{\epsilon - \sin^2 \theta}}, \quad (13)$$

$$T_s = \frac{2 \cos \theta}{\cos \theta + \sqrt{\epsilon - \sin^2 \theta}}, \quad (14)$$

where $F(\omega) = \sqrt{1 - \sin^2 \theta / \epsilon(\omega)}$.

IV. RESULTS AND DISCUSSION

A. Atomic and electronic structure

Atomic geometries of the GaN(0001) surface are optimized through calculations of atomic forces which contain both the Hellmann-Feynman and the Pulay correction terms.⁴¹ Here we consider two atomic configurations: N-terminated (1×1) structure, and Ga-terminated (1×1) surface where additional adatoms of Ga are placed directly over the surface nitrogen atoms. In agreement with previous finding,^{42,43} the Ga-terminated geometry is preferred energetically. Our value of 2.08 Å for the atomic bond length between adsorbed and host atoms of Ga-on-top geometry, is in a good agreement with the recent finding of 2.06 Å.⁴⁴

The calculated surface band structures of the Ga- and N-terminated GaN(0001)(1×1) surfaces are presented in Fig. 1. Significant differences are obvious between the two cases. The N-terminated GaN(0001)(1×1) surface has one dangling bond per unit cell. The π interaction between adja-

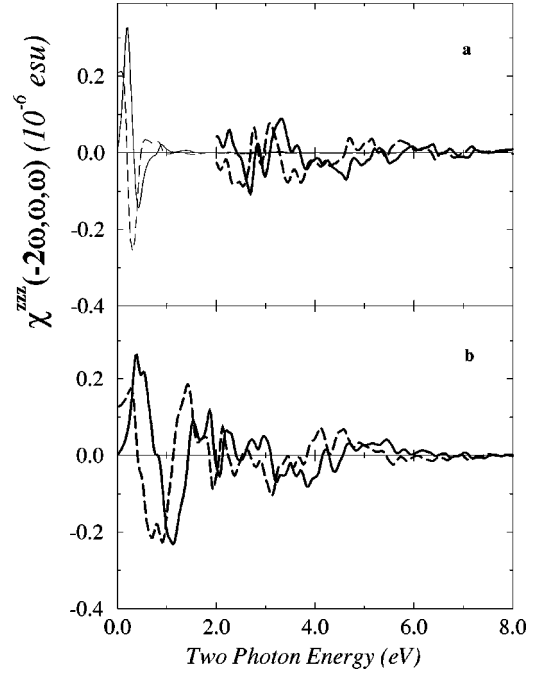


FIG. 2. The calculated spectra of the second-order optical susceptibility component $\chi_{zzz}^{(2)}(-2\omega, \omega, \omega)$ of the N-terminated (a) and Ga-terminated (b) GaN(001)(1×1) surfaces (bold solid lines). The real and imaginary parts are shown by dashed and solid lines, respectively. The rescaled (by factor 1/40) spectra are shown in panel (a) by the thin lines.

cent dangling bonds is responsible for the metallic character of this surface. The electronic structure of this surface has well pronounced low dispersive metallic surface state in the gap [see Fig. 1(a)].

The Ga-terminated GaN(0001)(1×1) surface is characterized by three surface states [labeled as G_1 , G_2 , and G_3 in Fig. 1(b)], which disperse strongly in the Brillouin zone, indicating the strong interaction between the neighboring surface atoms. Our FLAPW band structure of the GaN(0001)(1×1):Ga surface confirms the previous results obtained from empirical calculations based on the extended Hückel method⁴⁵ and also most recent *ab initio* pseudopotentials study.⁴⁴

B. Nonlinear optical susceptibilities

The wurtzite GaN crystals are polar; the dipole second-order optical response is thus allowed in volume. An *ab initio* study of SHG in bulk GaN, using the FLAPW local-density approximation (LDA) theory, has been performed by Hugh, Wang, and Sipe in (Ref. 33). SHG spectra of all independent bulk components of $\chi^{(2)}$ in GaN are given in our recent study.¹⁶ To understand the contributions to $\chi^{(2)}$ from the surface states, it is instructive to compare results of two surfaces with substantially different electronic structures: the Ga- and N-terminated GaN(0001)(1×1) surfaces.

In this study we mostly concentrate on the SHG efficiencies rather than each individual component. In order to illustrate the typical behavior, the spectra of real and imaginary parts of $\chi_{zzz}^{(2)}$ are shown in Fig. 2. The absolute values of the all three independent components of $\chi^{(2)}$ calculated in this

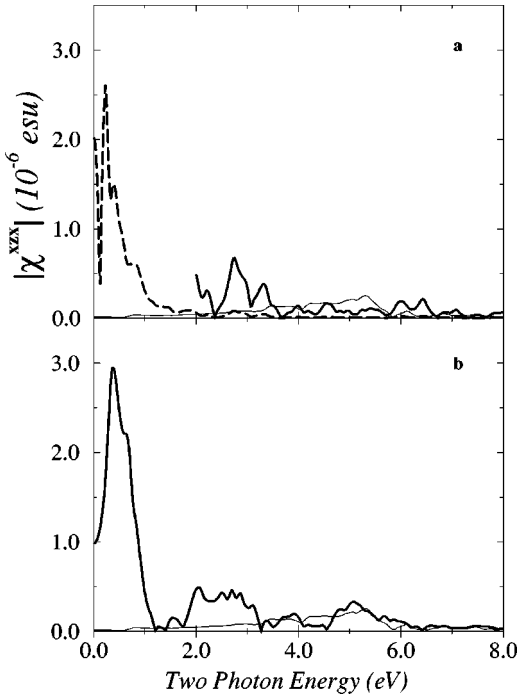


FIG. 3. The calculated spectra of absolute values of the second-order optical susceptibility component $\chi_{xzx}^{(2)}(-2\omega, \omega, \omega)$ of the N-terminated (a) and Ga-terminated (b) GaN(0001)(1×1) surfaces (bold solid lines). The thin solid lines the SHG spectra present results of the bulk wurtzite GaN (Ref. 16). The rescaled (by factor 1/8) surface spectrum is also shown in panel (a) by the dashed line.

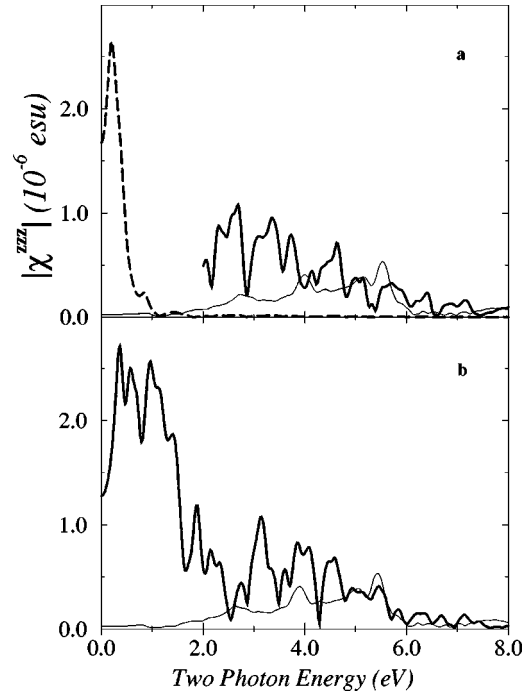


FIG. 5. The same as Fig. 3 but for $\chi_{zzz}^{(2)}(-2\omega, \omega, \omega)$ component. The rescaled (by factor 0.02) surface spectrum is also shown in panel (a) by the dashed line.

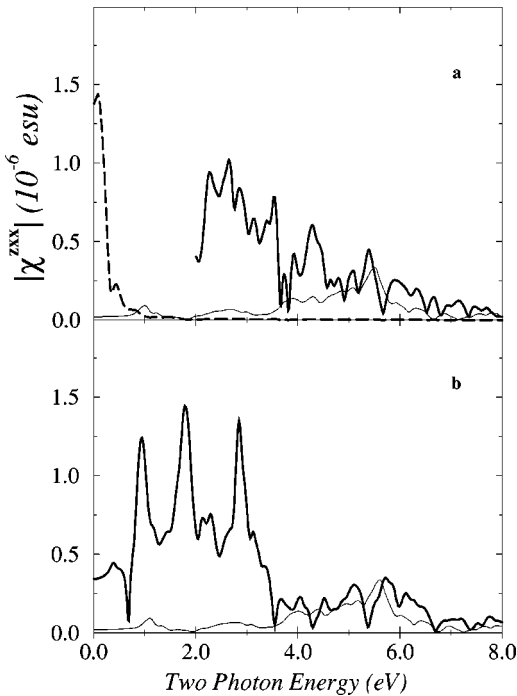


FIG. 4. The same as Fig. 3 but for the $\chi_{zxx}^{(2)}(-2\omega, \omega, \omega)$ component. The rescaled (by factor 0.01) surface spectrum is also shown in panel (a) by the dashed line.

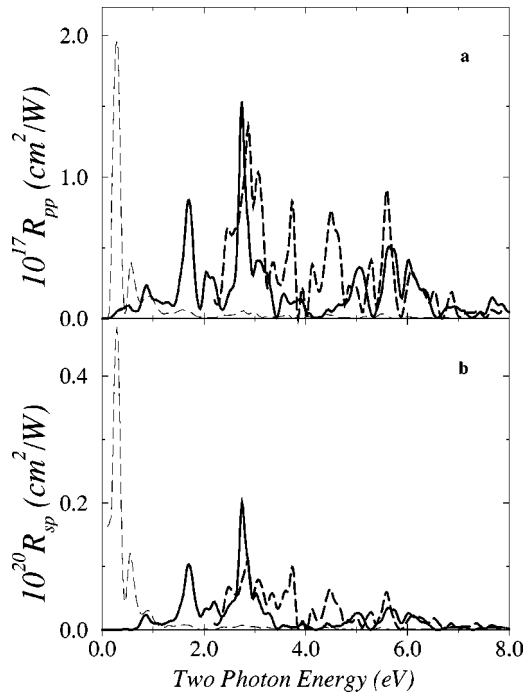


FIG. 6. SHG efficiencies for the *p*-in/*p*-out, R_{pp} (a) and the *s*-in/*p*-out, R_{sp} (b) configurations of GaN(0001)(1×1):Ga (solid lines) and of GaN(0001)(1×1):N (dashed lines) surfaces. The rescaled spectra (by a factor of 1/25) of the GaN(0001)(1×1):N surface are shown by the thin dashed lines. Note different scales in panels *a* and *b*.

work are presented in Figs. 3–5. The SHG efficiencies for p -in/ p -out (R_{pp}) and s -in/ p -out (R_{sp}) configurations are presented in Fig. 6.

Compared to the bulk functions in Ref. 16 (see the thin lines in Figs. 3–5), the SHG spectra can be separated into two spectral regions: region 1 ($0 \leq \hbar\omega \leq 5.0$ eV) and region 2 ($\hbar\omega > 5.0$ eV). In region 2 the SHG functions for both surfaces are obviously determined by the bulk responses (see Figs. 3–5). The R_{pp} and R_{sp} of both surfaces (see Fig. 6) converge to each other at $\hbar\omega > 5.0$ eV. The differences still seen in Fig. 6 are caused by the restrictions of the model. For thicker slab (with 16 ML's and more) the values of R_{pp} (R_{sp}) at $\hbar\omega > 5.0$ eV of both surfaces become quantitatively the same. In region 1, the calculated SHG functions appear to be dominated by contributions from the surface states.

Note that highly intensive peaks are predicted in the low-energy region for the N-terminated GaN(0001)(1×1) surface. Although the predicted peak intensities should be viewed cautiously as discussed in in Sec. III c, such strong peaks (rescaled in Figs. 2–6) promise a possibility to identify surface chemical compositions and atomic arrangements with an extremely high sensitivity.

Experimental SHG spectra of GaN(0001) surface are reported in Refs. 10 and 46. A surface-induced SHG peak near 2.8 eV was observed.⁴⁶ As discussed in Sec. III, for comparison with experiment the calculated SHG data should be corrected by Δ_{QP} . The best value of Δ_{QP} is 1.4 eV to match the measured gap of the bulk wurtzite GaN. Although it is not

clear what should be used for Δ_{QP} at surface, it is reasonable to assign the peak in the calculated spectra at 1.5–1.6 eV as the correspondent for the observation. A much stronger signal should be detected in the infrared-red spectrum region for the N-terminated GaN(0001) surface.

V. CONCLUSIONS

The atomic geometries, electronic band structures, and nonlinear optical functions of GaN(0001) surface are studied by using the *ab initio* FLAPW method. The Ga-terminated GaN(0001)(1×1) geometry is found to be more favorable energetically than the N-terminated surface. The surface specific features in the SHG nonlinear optical spectra are much stronger than the bulk responses. Nitrogen termination strongly enhances the surface contribution to SHG spectra of the GaN(0001) surface in the low-energy spectrum region, whereas adsorption of a Ga monolayer reduces it in relation to nitrogen. This result can be used as a highly sensitive *in situ* tool to monitor the changes in chemical composition and geometry during the growth processes.

ACKNOWLEDGMENTS

W. E. Angerer is acknowledged for providing his Ph.D. thesis. Work supported by the Division of Chemical Science, office of Basic Energy Science, U.S. Department of Energy (Grant No. DE-FG03-99ER14948) and by a computing grant at NERSC.

-
- ¹*Properties of Group III Nitrides*, edited by J. H. Edgar (EMIS Data Reviews Series, London, 1994).
- ²S. C. Jain, M. Willander, J. Narayan, and R. Van Overstraeten, *J. Appl. Phys.* **87**, 965 (2000).
- ³G. Lüpke, *Surf. Sci. Rep.* **35**, 75 (1999).
- ⁴J. R. Power, J. D. O'Mahony, S. Chandola, and J. F. McGilp, *Phys. Rev. Lett.* **75**, 1138 (1995).
- ⁵C. Meyer, G. Lüpke, U. Emmerichs, F. Wolter, H. Kurz, C. H. Bjorkman, and G. Lucovsky, *Phys. Rev. Lett.* **74**, 3001 (1995).
- ⁶U. Höfer, *Appl. Phys. A: Mater. Sci. Process.* **63A**, 533 (1996).
- ⁷M. C. Downer, *Bull. Am. Phys. Soc.* **45**, 720 (2000).
- ⁸J. I. Dadap, Z. Xu, X. F. Hu, M. C. Downer, N. M. Russell, J. G. Ekerdt, and O. A. Aktsipetrov, *Phys. Rev. B* **56**, 13 367 (1997).
- ⁹A. Liu, S.-L. Chuang, and C. Z. Ning, *Appl. Phys. Lett.* **76**, 333 (2000).
- ¹⁰W. E. Angerer, N. Yang, A. G. Yodh, M. A. Khan, and C. J. Sun, *Phys. Rev. B* **59**, 2932 (1999).
- ¹¹R. Del Sole and A. Selloni, *Phys. Rev. B* **30**, 883 (1984).
- ¹²B. Mendoza, A. Gaggiotti, and R. Del Sole, *Phys. Rev. Lett.* **81**, 3781 (1998).
- ¹³V. I. Gavrilenko and F. Rebrost, *Appl. Phys. A: Mater. Sci. Process.* **60A**, 143 (1995); *Surf. Sci.* **331-333**, 1355 (1995).
- ¹⁴D. Lim, M. C. Downer, J. G. Ekerdt, N. Arzate, B. S. Mendoza, V. I. Gavrilenko, and R. Q. Wu, *Phys. Rev. Lett.* **84**, 3406 (2000).
- ¹⁵V. I. Gavrilenko, R. Q. Wu, M. C. Downer, J. G. Ekerdt, D. Lim, P. Parkinson, *Thin Solid Films* **364**, 1 (2000).
- ¹⁶V. I. Gavrilenko and R. Q. Wu, *Phys. Rev. B* **61**, 2632 (2000).
- ¹⁷E. Wimmer, H. Krakauer, M. Weinert, and A. J. Freeman, *Phys. Rev. B* **24**, 864 (1981), and references therein.
- ¹⁸D. D. Koelling and B. N. Harmon, *J. Phys. C* **10**, 3107 (1977).
- ¹⁹J. P. Perdew, K. Burke, and Y. Wang, *Phys. Rev. B* **54**, 16 533 (1996).
- ²⁰V. I. Gavrilenko and F. Bechstedt, *Phys. Rev. B* **55**, 4343 (1997).
- ²¹M. S. Hybertsen and S. G. Louie, *Phys. Rev. B* **34**, 5390 (1986); **35**, 5585 (1987).
- ²²M. P. Surh, S. G. Louie, and M. L. Cohen, *Phys. Rev. B* **43**, 9126 (1991).
- ²³A. S. Davydov, *Solid State Theory* (Academic Press, New York, 1980).
- ²⁴D. E. Aspnes, *Phys. Rev. B* **6**, 4648 (1972).
- ²⁵Z. H. Levine and D. C. Allan, *Phys. Rev. B* **42**, 3567 (1990); **43**, 4187 (1991); **44**, 12 781 (1991).
- ²⁶R. Del Sole and R. Giralanda, *Phys. Rev. B* **48**, 11 789 (1993).
- ²⁷N. Bloembergen, *Nonlinear Optics* (Benjamin, New York, 1965).
- ²⁸A. Liebsch, *Electronic Excitations at Metal Surfaces* (Plenum Press, New York, 1997).
- ²⁹Y. R. Shen, *The Principles of Nonlinear Optics* (Wiley, New York, 1984).
- ³⁰B. Adolph and F. Bechstedt, *Phys. Rev. B* **57**, 6519 (1998).
- ³¹J. E. Sipe and E. Ghahramani, *Phys. Rev. B* **48**, 11 705 (1993).
- ³²J. L. P. Hughes and J. E. Sipe, *Phys. Rev. B* **53**, 10 751 (1996).
- ³³J. L. P. Hughes, Y. Wang, and J. E. Sipe, *Phys. Rev. B* **55**, 13 630 (1997).

- ³⁴N. Blombergen, R. K. Chang, S. S. Jha, and C. H. Lee, Phys. Rev. **174**, 813 (1968).
- ³⁵P. Guyot-Sionnest, W. Chen, and Y. R. Shen, Phys. Rev. B **33**, 8254 (1986).
- ³⁶J. Chen, L. Jönsson, J. W. Wilkins, and Z. H. Levine, Phys. Rev. B **56**, 1787 (1997).
- ³⁷O. A. Aktsipetrov, A. A. Fedjanin, J. I. Dadap, and M. C. Downer, Laser Phys. **6**, 1142 (1996).
- ³⁸J. I. Dadap, J. Sham, A. S. Weling, J. A. Misewich, and T. F. Heinz, Appl. Phys. B: Lasers Opt. **68B**, 333 (1999).
- ³⁹B. S. Mendoza and W. L. Mochan, Phys. Rev. B **55**, 2489 (1997).
- ⁴⁰J. E. Sipe, D. J. Moss, and H. M. van Driel, Phys. Rev. B **35**, 1129 (1987).
- ⁴¹R. Wu and A. J. Freeman, Phys. Rev. B **51**, 17 131 (1995).
- ⁴²A. R. Smith, R. M. Feenstra, D. W. Greve, J. Neugebauer, and J. E. Northrup, Phys. Rev. Lett. **79**, 3934 (1997).
- ⁴³J. Fritsch, O. F. Sankey, K. E. Schmidt, and J. B. Page, Phys. Rev. B **57**, 15 360 (1998).
- ⁴⁴F.-H. Wang, P. Krüger, and J. Pollmann, Phys. Rev. B **64**, 035305 (2001).
- ⁴⁵T. Strasser, C. Solterbeck, F. Starrost, and W. Schattke, Phys. Rev. B **60**, 11 577 (1999).
- ⁴⁶W. E. Angerer, Ph.D. thesis, University of Pennsylvania, 1998.